H1-07/91-186

16.07.91

QUASI-REAL QED COMPTON AT HERA

by

A. COURAU
Laboratoire de l'Accélérateur Linéaire
CNRS - IN2P3 - Université de Paris-Sud
91405 ORSAY France

INTRODUCTION

This note is divided as follows :

In the first part we will give the main definitions and some general remarks about the quasi-real QED Compton process and its experimental interest.

In the second part we will first discuss this process initiated by a Dirac particle (namely $ee \rightarrow (e)e\gamma$). This corresponds to a pure QED process exactely computable and which provides us with some general features.

Then in the third part we will study the Compton process at HERA describing in some details the various contributions and the underlying assumptions.

In the last part, we will try to show in a very clear way, the main characteristics and their main corrections.

All those discussions will be illustrated by figures obtained through the Monte-Carlo generator.

I - DEFINITIONS AND REMARKS

Considering the reaction $ep \rightarrow e\gamma X$ corresponding to the diagram

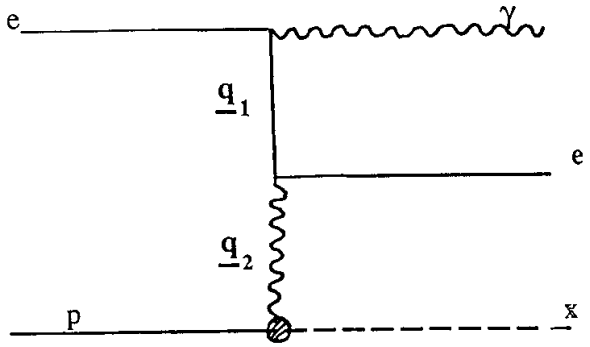

one gets, a priori*

$$ds \approx \frac{dq_1}{q_1^2 - m_e^2} \cdot \frac{dq_2}{q_2^2}$$

It results that the cross section is largely dominated by both q^2 close to zero. But in this case the outgoing electron and photon, as well as the hadronic system, go along the beam axis and escape the main detector. This configuration corresponds to the so-called **Bremβtrahlung**. It leads to a large counting rate, but only in a specific detector for low angles.

Looking for particles at finite angles inside the detector requires at least that one of the two q^2 takes finite values not too close to zero. Then the cross section will be dominated by the other q^2 close to zero. One shall thus consider two different configurations :

i) $q_1^2 \rightarrow 0$, q_2^2 finite : then the photon goes staightforward along the incident electron direction, and we observe in the detector the electron and the hadronic system. This corresponds to the so-called **radiative correction** .

ii) $q_2^2 \rightarrow 0$, q_1^2 finite : then the hadronic system goes straightforward, and we observe in the detector the electron and the photon . This corresponds to the so-called **quasi-real Compton** process.

Those various configurations are shown schematically in the following Table.

---

* Let us note that in practice the pole in the propagator of the exchanged photon vanishes when both vertices $e\gamma e$ and $p\gamma X$ are inelastic

	experimental configuration	observed at large angle	so call
$q_1^2 \to 0$ $q_2^2 \to 0$	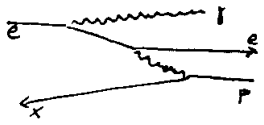		Bremβtrahlung
$q_1^2 \to 0$	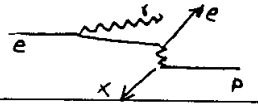	e X	radiative correction
$q_2^2 \to 0$	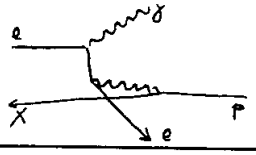	e γ	quasi real compton

We call quasi-real QED COMPTON those experimental events that involve one electron and one photon observed in the detector (at finite angle γ) since they are dominated by small q_2^2 and thus they involve the scattering of a quasi-real γ with the incident electron. Notice that small q_2^2 actually means small with respect to W^2 where W is the invariant mass of the eγ system.
A priori one selects events with $|q_2^2| << W^2$ by looking at coplanar eγ events observed within the detector.

Thus assuming "HEAD-ON eγ COLLISIONS" $|\Sigma \vec{Pt}| = 0$ it results the following consequences :

There are only 3 free parameters e.g. : E_γ, $\cos\theta^*$, ϕ^* where Eγ is the energy of the quasi-real photon in the Lab. frame and θ^* φ^* the orbital and azimuthal angle of the outgoing photon in the C-of-M frame.

There are 6 measured quantities $(E' \Theta \phi)_e$ $(E' \Theta \phi)_\gamma$ where E' are the energies and Θ, φ the orbital and azimuthal angles of the outgoing particles (e, γ) in the lab. frame.

Therefrom one gets very strong constraints, and those constraints make this process very well suited for electromagnetic calibration of the detector

Moreover those events appear with a fairly large counting rate ; they can be very easely separated from any background and they involve large visible Energy (Evis > E_e). All this makes them suited, as well, for measurement of the luminosity within the detector.

It should also be noticed that the quasi-real Compton process has a very good sensitivity to a possible exited electron e* created in the s channel[1].

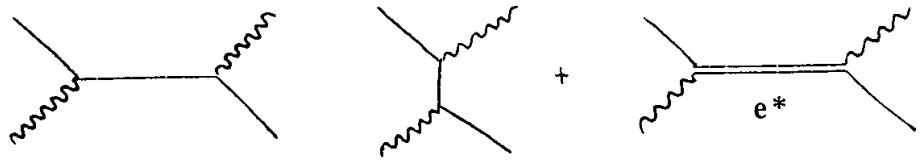

The same process exists as well in e^+e^- collisions, i.e. $e^+e^- \rightarrow e^+e^-\gamma$:

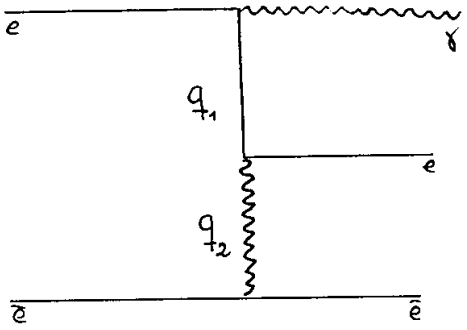

$q_1^2, q_2^2 \rightarrow$ Bremβtrahlung.

$q_1^2 \rightarrow 0$ radiative Bhabha

$q_2^2 \rightarrow 0$ " quasi-real Compton"

It has been already observed many years ago at ACO[2]. Since then, it has been studied experimentally in order to provide limits on the coupling of a possible e* at PEP[3], PETRA[4] and TRISTAN[5]. In addition, there exists new results from LEP up to invariant masses around 100 GeV. This is a pure QED process. We have provided exact Monte-Carlo generator for that process many years ago[1 - 3].

But $pe \rightarrow Xe\gamma$, at HERA, involves important difference :

i) There is only one electron beam

ii) The proton mass is 200 times the mass of the electron

iii) The energies of the incident beams are different $Ep \simeq 30\, Ee$

iii) The proton is not a pointlike Dirac particle : it has an anomalous magnetic moment, electromagnetic form factors, and inelastic contributions. Therefore the computations are partly model-dependant, and exact expression of the cross section cannot be provided.

This model-dependence entails two main consequences :

i) for luminosity measurements, where great precision is required, experimental cuts must be defined in order to minimize possible inaccuracies.
ii) on the other hand, it is particularly interesting to study those kinematic regions where uncertainties due to to the theoretical models used are large ; experimental measurements will thus provide us with a test of those models, and actually with the "photon structure of the proton".

For simplicity, we will first discuss Compton process initiated by a pure Dirac particle, i.e. the corresponding configuration of $e\bar{e} \rightarrow (e)\bar{e}\,\gamma$ which will provide us with some general features. We will then go over to the Compton process at HERA, (i.e. for $ep \rightarrow (x)\,e\gamma$) , which is somewhat more complicated.

II - COMPTON SCATTERING IN e^+e^- COLLISIONS

Using an exact computation based on helicity amplitudes one gets :

$$\frac{d\sigma^{e\bar{e}\rightarrow e\gamma e}}{dy\,dQ^2\,d\Omega^*} = f_{\gamma^*/e}(y,Q^2)\,\frac{d\sigma^{\gamma^*\bar{e}\rightarrow\gamma\bar{e}}}{d\Omega^*}$$

$$f_{\gamma^*/e}(y\,Q^2) = \frac{\alpha}{\pi y}\left[(1-y+y^2/2)\frac{1}{Q^2} - (1-y)\frac{Q^2_{min}}{Q^4}\right]$$

$$\frac{d\sigma^{\gamma^* e\rightarrow\gamma e}}{d\Omega^*} = \frac{d\sigma_T}{d\Omega^*} + \varepsilon\frac{d\sigma_L}{d\Omega^*} + \sqrt{2\varepsilon(1+\varepsilon)}\,\frac{d\sigma_{TL}}{d\Omega^*}\cos(\varphi^*) + \varepsilon\frac{d\sigma_{TT}}{d\Omega^*}\cos(2\varphi^*)$$

$$\frac{d\sigma_T}{d\Omega^*} = \frac{\alpha^2}{4(W^2+Q^2)}\left[\frac{4W^2}{(W^2+Q^2)(1+u^*+\eta)} + \frac{(W^2+Q^2)(1+u^*)}{W^2} + \frac{4Q^2}{W^2}\frac{(1-u^*)}{(1+u^*-\eta)} + \frac{2Q^2(1-u^*)}{W^2+Q^2}\right]$$

$$\frac{d\sigma_L}{d\Omega^*} = \frac{\alpha^2}{W^2+Q^2}\left[\frac{Q^2(1-u^*)}{W^2+Q^2}\right]$$

$$\frac{d\sigma_{TL}}{d\Omega^*} = -\frac{\alpha^2}{W^2+Q^2}\,\frac{QW}{2(W^2+Q^2)}\left[\sqrt{1-u^*} + \frac{Q^2}{W^2}\,\frac{1-u^*}{1+u^*+\eta}\right]$$

$$\frac{d\sigma_{TT}}{d\Omega^*} = \frac{\alpha^2}{W^2+Q^2}\,\frac{Q^2}{2(W^2+Q^2)}(1-u^*)$$

with : $y = \frac{W^2 + Q^2}{s}$ $\varepsilon = \frac{1 - y}{1 - y + y^2/2}$ $\eta = \frac{2\, m_e\, W^2}{(W^2 + Q^2)^2}$

where Q^2 is the absolute values of the four momentum squared of the virtual photon γ^*;W is the invariant mass of the outgoing $e\gamma$ System ; s is the total energy squared of the overall reaction $u^* = \cos\theta^*$ $d\Omega^* = d\cos\theta^* d\varphi^*$ are defined in the $\gamma^* e \rightarrow \gamma e$ center of mass frame.

Equivalent photon approximation (E.P.A.).

For$Q^2 \ll W^2$, neglecting terms in Q^2/W^2, we still remain with :

$$\frac{d\sigma^{e\bar{e}\rightarrow e\gamma e}}{dy\, dQ^2\, d\Omega^*} = f_{\gamma^*/e}(y,Q^2)\, \frac{d\sigma^{\gamma^*\bar{e}\rightarrow\gamma\bar{e}}}{d\Omega^*}$$

$$f_{\gamma^*/e} = \frac{\alpha}{\pi y}\left[(1 - y + y^2/2)\frac{1}{Q^2} - (1 - y)\frac{Q^2_{min}}{Q^4}\right]$$

but the expression of $\frac{d\sigma^{\gamma^* e\rightarrow\gamma e}}{d\Omega}$ is considerably simplified, i.e. :

$$\frac{d\sigma^{\gamma e\rightarrow\gamma e}}{d\Omega^*} = \frac{\alpha^2}{4\pi^2}\left[\frac{4}{1 + u^* + \eta} + 1 + u^*\right]$$

while the expressions of y and η are simplified as well :

$$y = \frac{W^2}{s} = \frac{E_\gamma}{E_{inc}} \qquad \eta = \frac{2m_e^2}{W^2}$$

Let us emphasize the following :

E.P.A. is only a dynamic approximation, that allows for a factorization of the cross section by neglecting certain terms ; but the distributions of all parameters (Q^2,W,u^*,φ^*) remain defined. It is very different from the approximation historically known as the "Williams-Weiz-Säcker formula", which contains an integration over Q^2 and assumes the quasi-real photon to be emitted at 0°.

Thus the events can be fully generated according to the E.P.A. and afterwords corrected by comparing the real exact differential cross section to the E.P.A. expression used in the generation. This allows us to provide an exact Monte Carlo over the whole space phase.

However the "weight" of the generated events becomes as much large than the Q^2/W^2 increases. Thus, in practice, we have advantage to limit the range of Q^2/W^2 of the experimental and generated events.

Let us note that when Q^2/W^2 increases, the main correction proceeds from the 2 terms which were initially neglected in $d\sigma_T/d\Omega^*$.

QED Monte-Carlo for ee $\rightarrow$ (e) e γ.

In a first step events are generated according to E.P.A. with radiative correction as shematically shown just below.

Radiative correction[6]

$$\frac{dN}{dk} = \beta \frac{1}{k^{1-\beta}}(1 - k + k^2) \qquad \text{with } \beta = \frac{2\alpha}{\pi}\left(\ln\frac{2E}{m_e} - \frac{1}{2}\right) \; ; \; k = E_\gamma/E$$

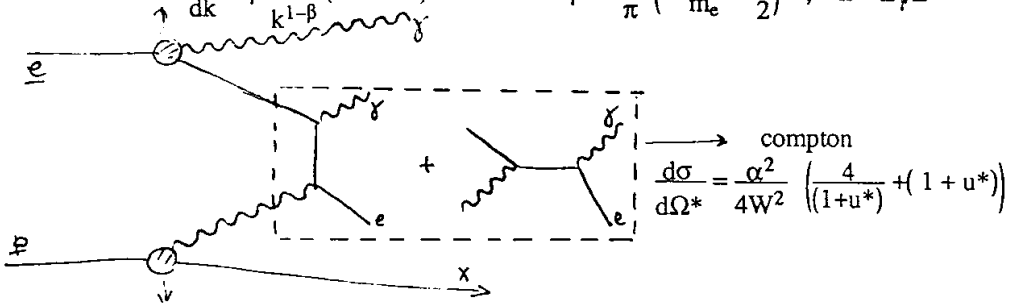

Equivalent Photon Approximation (E.P.A.)

$$\frac{dN}{dy\,dQ^2} = \frac{a}{\pi y}\left[(1 - y + y^2)/2)\frac{1}{Q^2} - (1-y)\frac{Q^2_{min}}{Q^4}\right] \qquad \text{with } y = W^2/s$$

The generation is performed over the whole experimentally available phase space that we must first determined. Thus we generate the Energy of the radiatif photon and deduce Ee the effective value of the Energy of the incident electron involved in the compton scattering. Then W, Q^2, Θ^* and φ^* are easily generated according to dW/W^3, dQ^2/Q^2, $du^*/(1 + u^*)$ and $d\varphi^*$, and slightly corrected. All kinematic parameters are derived and taken into account in an exact way.

One event being generated with all defined parameters one compares the real differential praobability of that event with the probability used in the first step of the Monte Carlo. Such Monte-Carlo is absolutely normalized.

III - QED COMPTON SCATTERING AT HERA : e p → e γ (X)

In 1984, we used the Dirac approximation (traiting the proton as a Dirac particle), with a sharp cut on $|\Sigma\vec{P_t}|/W$. We assume indeed that at least for Q^2 not too large, the inelastic contribution compensates more or less the drop in the elastic one, due to the electromagnetic form factors. This procedure provides the correct order of magnitude.

In 1990, we perform a complete Monte-Carlo. The elastic contribution makes no problem using conventional expressions of the electromagnetic form factors. However the inelastic contribution is somewhat model-dependent (see hereafter).

That Monte-Carlo was run early in 1990 and put into H1 shape by T. Carli. It performs an analytic integration over x (i.e. over the hadronic masses).

In 1991, a new version of the Monte-Carlo (not yet in H1 shape) includes as well the generation of x (resp. W_H). Actually it makes no difference with the previous one and does not present a real advantage as far as H1 is concerned.

1. For the elastic contribution $e\,p \rightarrow e\,\gamma(p)$ *, one gets :*

$$\frac{d\sigma^{ep\rightarrow e\gamma(x)}}{dy\,dQ^2\,d\Omega^*} = f_{\gamma^*/p}(y,Q^2)\,\frac{d\sigma^{\gamma^* e\rightarrow \gamma e}}{d\Omega^*}$$

$$f_{\gamma^*/p} = \frac{a}{\pi y}\left[(1-y)\frac{Q^2-Q^2_{min}}{Q^4}\left[\frac{G_E^2+\tau\,G_M^2}{1+\tau}\right]+\frac{y^2}{2}\frac{1}{Q^2}G_M^2\right]$$

with $G_E = \frac{G_M}{2.79} = \left[1+\frac{Q^2(GeV^2)}{0.71}\right]^{-2}$

and $\tau = Q^2 / 4\,M_p^2$

with :

$$Q^2_{min} = \frac{y_0^2}{1-y_0}M^2 \quad \text{with} \quad y_0 = \frac{W^2}{s} = \frac{E\,\gamma}{E_p}$$

$$y = \frac{W^2+Q^2}{s} \qquad \text{with} \quad s = 4\,E_e\,E_p$$

$$\text{let us note : } y = \frac{W^2+Q^2}{s} = \frac{\underline{e}\,\underline{\gamma}}{\underline{e}\,\underline{p}}$$

Remember that for a Dirac particle, one has :

$$f_{\gamma^*/p} = \frac{\alpha}{\pi y}\left[(1-y)\frac{Q^2 - Q^2_{min}}{Q^4} + y^2/2\,\frac{1}{Q^2}\right]$$

so that at small Q2 the elastic contribution remains the same as the one given by the DIRAC approximation.That contribution is practically confined in the range :

$$\frac{W^4}{s}\frac{M^2}{s - W^2} \leq Q^2 \leq 1\ \text{GeV}^2$$

2. For the inelastic contribution $e\,p \rightarrow (H)\,e\,\gamma$

Assuming $\sigma_L = Q^2/\nu^2\ \sigma_T$ with $\nu = \dfrac{W_H^2 - M_p^2 + Q^2}{2\,M_p}$ where W_H is the hadronic mass produced, one gets :

$$\frac{d\sigma^{pe = He\gamma}}{dx\,dy\,dQ^2\,d\Omega^*} = [F(x)/x]\left[f_{\gamma^*/p}(y/x\ ,\ Q^2)\right]\frac{d\sigma^{\gamma^* e \rightarrow \gamma e}}{d\Omega^*}$$

where $\quad x = \dfrac{Q^2}{Q^2 + W_H^2 - M_p^2} \quad y = \dfrac{W^2 + Q^2}{s} \quad (s = 4\,E_e\,E_p)$

$$f_{\gamma^*/p} = \frac{\alpha\,x}{\pi\,y}\left[(1-y/x)\frac{Q^2 - Q^2_{min}}{Q^4} - \frac{y^2}{2\,x^2}\frac{1}{Q^2}\right]$$

$$Q^2_{min} = M_p^2\,\frac{y^2}{1 - y/x}$$

That inelastic contribution can be derived directly from the quark parton model (with $F(x) = F_2^p(x)$ the classical F_2 structure function of the proton). However that model is valid only for somewhat large values of W_H and Q^2.

On the other hand, we know that there exists an inelastic cross section due to real photoproduction ($\gamma p \rightarrow H$) the experimental values of which are well known, as well as the electroproduction cross section of the 3 first resonances. Thus the inelastic contributions were derived considering various regions of W_H and Q^2.

b.1 - For $(M_p + m_\pi) \leq W_H \leq 2$ GeV, i.e. for :

$$\frac{Q^2(GeV^2)}{Q^2(GeV^2) + 3} \leq x \leq \frac{Q^2(GeV^2)}{Q^2(GeV^2) + 0.3}$$

we know from photoproduction and electroproduction that this region is essentially saturated by the production of the three resonances Δ (1236), N* (1520) and N* (1688) . Then we set *

$$F(x) = \sigma_t \frac{Q^2}{4\pi^2\alpha}$$

$$\sigma_t = \sigma_0 \frac{W_R^2\,\Gamma^2}{\left(W_H^2 - W_R^2\right)^2 + W_R^2\,\Gamma^2}\left(1 + \frac{Q^2}{Q_t^2}\right)^2$$

where we use the following experimentally known values for the various parameters.

	Δ	N *	N *
W_R (GeV/c)	1236	1520	1688
Q^2t (GeV^2)	2.5	3.0	3.0
Γ (GeV)	0.12	0.12	0.12
σ (μb)	550	280	220

* Let us note that the relations $\sigma_L = (Q^2/\nu^2)$. σ_L is not here justified, so that a correct determination from the experimental known results must be slightly different.

b.2 - For $W_H \geq 2$ GeV, i.e. for :

$$\frac{W^2 + Q^2}{s} \leq x \leq \frac{Q^2(GeV^2)}{Q^2(GeV^2) + 3}$$

we proceed as follows :

i) for Q^2 large enough, we assume the quark-parton Model to be valid, so that one has $F(x) = F_2^p(x)$

ii) for $Q^2 \rightarrow 0$ F(x) is derived from the experimental total photoproduction cross section which is known to be approximately constant $\left(\sigma_{\gamma p} \approx 120_{\mu b} \text{ for } W_H > 2GeV\right)$, then one gets :

$$F(x) = \frac{Q^2}{4\pi^2\alpha} \sigma_{\gamma p} \sim Q^2(GeV^2)$$

iii) for the whole Q^2 range ; one assumes some continuity between the two Q2 regions. Thus we perform an interpolation in the intermediate range using in the whole range the following expression :

$$F(x) = F_2^p(x) \frac{Q^2(GeV^2)}{Q^2(GeV^2) + F_2^p(x)}$$

so that :

when $Q^2(GeV2) >> F_2^p(x)$, F(x) tends to $F_2^p(x)$

when $Q^2(GeV2) >> F_2^p(x)$, F(x) tends to Q^2

Noticing that in the x range involved $(F_2^p(x)$ remains of the order of 0.2.

The overall results from the Monte-Carlo within some "typical" conditions (namely $3.6 \leq \Theta \leq 176$ degrees ; $|\pi - \Delta\phi| \leq 45$ degrees ; E'_γ, $E'_e < 1$ GeV ; Eg + Ee > 20 GeV ; $|\Sigma \vec{Pt}| < 100$ GeV) are shown in Table 1 and figures 1 to 4. The influence of cuts and the very different "regime" of this process in various domains will be discuss and illustrate hereafter.

IV - MAIN CARACTERISTICS

- KINEMATIC

In first approximation, for $Q^2 \rightarrow 0$ there are head on γe collisions and thus neglecting the transverse momentum of the $e\gamma$ system, radiative correction and Masses of particles (i.e. using the W.W. Approximation), one gets :

$$E_{vis} = Ee + E\gamma$$

$$W^2 = 4.Ee.E\gamma$$

$$\beta = (E\gamma - Ee)/(Ee + E\gamma)$$

where E_e is the well known energy of the incident electron ; E_γ the energy of the quasi real photon which is the only free parameter, let us note that :

$\beta < 0$ i.e. $\vec{\beta}$ parallel to the incident electron for $E\gamma < 30$ Gev $W < 60$ GeV
$\beta = 0$ for $E\gamma = 30$ Gev $W = 60$ GeV
$\beta > 0$ i.e. $\vec{\beta}$ parallel to the incident proton for $E\gamma > 30$ GeV $W > 60$ GeV

On the other hand, calling E'_e, E' the energies of the outgoing particles, one has :

$$Evis = E'e + E'\gamma$$

$$W^2 = 2E'eE'\gamma\,(1 - \cos(\Theta e + \Theta\gamma))$$

$$\beta = \sin(\theta\gamma + \Theta e) / (\sin \Theta e) + \sin \Theta\gamma)$$

$$\cos\Theta e = (\cos\theta^* - \beta)/(1 - \beta \cos\theta^*) \quad ; \quad \Theta e = \pi + \varphi^*$$

$$\cos\Theta\gamma = (\beta - \cos\theta^*)/(1 + \beta \cos\theta^*) \quad ; \quad \Theta\gamma = \varphi^*$$

where θ^* φ^* and Θ, φ are the orbital and azimutal angles of the outgoing $e\gamma$ respectively in the C-of-M frame and in the Laboratory.
Therefrom, we get the following constraints :

$$E\gamma/Ep = W^2/S = (Evis - Ee)/Ep = [(1-\beta)/(1+\beta)] .Ee/Ep$$

$$Ee/\sin\Theta\gamma = E\gamma/\sin\Theta e = 2\,Ee/(\sin\Theta e + \sin\Theta\gamma - \sin(\Theta e + \Theta\gamma))$$

$$\Delta(\phi) \rightarrow \pi \quad |\Sigma \vec{Pt}| \rightarrow 0$$

As examples of the accuracy of those approximations; fig. 5 shows the $\Delta(\phi)$ distribution and the correlations beetwen W, E_{vis} and the direction of $\vec{\beta}$, obtained from the complete Monte-Carlo (without radiative correction).

- DYNAMIC

Again, in first approximation the overall differential cross section is the convolution of

i) the radiated photon spectrum $\propto (dE\gamma/E\gamma)\ (dQ^2/Q^2)$
ii) and the $e\gamma \rightarrow e\gamma$ cross section $\propto (1/W^2)\ (du^*/(1+u^*))$.

One concludes :

i) Regarding the W dependance since $W^2 = 4EeE\gamma$ one gets, $dE\gamma/E\gamma = dW/W$ or $1/W2 = 1/E\gamma$, thus $d\sigma \propto dW/W^3 = dE\gamma/E\gamma^2$.

ii) Regarding the Q^2 dependance, we notice that in practice, the elastic and the inelastic contribution are very different, the pole on Q^2 disappears for the inelastic contribution when the elastic contribution vanishes for Q^2 above 1 GeV^2.

iii) Regarding the u* dependence, we notice the backward pole in the compton scattering.

- SOME NUMERICAL VALUES

When $E\gamma < Ee$, i.e. β along the incident electron direction, if $E\gamma$ decreases, $|\beta| = (E_e - E_\gamma)(E_e + E_\gamma)$ increases while Ω^* the angular acceptance in the C-of-M frame decreases.
Thus the maximum value of $|\beta|$ is given by the limitation on Ω^* and one has :

$$|\beta|_{MAX} = |\cos \Theta_0|$$

where Θ_0 is the maximal angle of the experimental acceptance of the detector in the LAB system. Therefrom one gets :

$$E_\gamma \geq (E_\gamma)_{MIN} = \frac{1 - |\cos \Theta_0|}{1 + |\cos \Theta_0|} E_e$$

and, for $\Theta_0 = 176$ degrees, $E_e = 30$ GeV and $E_p = 820$ GeV, one obtains :

$(E_\gamma)_{min} = 0.036$ GeV $\quad (E_\gamma)_{min}/E_p \sim 4\ 10^{-5}$

$W_{min} \sim 4\ (E_\gamma)_{min}\ E_p \simeq 2$ GeV

$$Q^2_{min} \sim \frac{W^4_{min}}{S} \frac{M_p^2}{S - W^2} \simeq 10^{-9} GeV^2$$

Some correlations and order of magnitudes of numerical values for an angular acceptance given in the Lab. by $|\cos\Theta| \leq 0.997$ are shown in the following table.

W(GeV)	2	10	60	100	200
E_γ(GeV)	0.036	0.83	30	83	333
$1/W^3$	10^{-1}	10^{-3}	$5\ 10^{-6}$	10^{-6}	10^{-7}
β	− 0.997	− 0.946	0	0.47	0.83
$\lvert\cos\theta^*\rvert$	~0	0.897	0.997	0.991	0.961
Q^2_{min}	10^{-9}	$6\ 10^{-7}$	10^{-4}	10^{-2}	0.16
$\int_{Q^2_{min}}^{1} dQ^2/Q^2$ "elastic"	21	15	9	5	2

The various contributions and distributions, actually observed through the Monte-Carlo, in the various range are shown in figures 6 to 11.

- MAIN CORRECTIONS

There are two significant corrections to the previous main caracteristics which are even very important at low W.

i) The first one is the radiative correction. This correction is mainly due to the radiation from the incident electron which reduces its effective incident energy E_e. High energy radiation has low probability by itself, but this low probability may be compensated by a large increase of the cross section due mainly to the decrease of W and to the change in β. Such effects are shown in figure 12 where the cut on the visible energy was relaxed in the Monte-Carlo. However we observed that actually the high energy radiation events can be eliminated through a cut on the visible energy as Evis > 20 GeV for example ; but then the observed cross section is significantly changed and it still remains some kinematical effects as observed for example when comparing figure 5 and figure 13.

ii) The second important correction is involved by the tail of Q2 values above Q^2_{min}. Actually the exact kinematic leads to :

$$W^2 = 4E_e E_\gamma - \left(1 - \frac{E_e}{E_p}\right) Q^2 \approx 4E_e E_\gamma - Q^2$$

$$\left(\Sigma \vec{p_t}\right)^2 = Q^2 \left(1 - \frac{W^2 + Q^2}{sx}\right) \approx Q^2$$

It results that, as Q^2 increases

i) W^2 increases

and, a fortiori,

ii) the virtuality Q^2/W^2 and thus the cross section increases,

iii) the $|\Sigma \vec{p_t}|/W$ ($\sim Q/W$) and thus the acoplanarity angle between outgoing e, γ increases.

Therefore a large amount of events at very small W comes from events where the value of Q^2 cannot be neglicted with respect to $4E_e E_\gamma$. Let us note that this can already occur at small Q^2. As an example, a Q^2 of the order of 1 GeV^2 shifts the previous minimal value of W from 2 GeV to 1 GeV.

However those events are caracterised by a large acoplanarity and a cut on this quantity is very efficient in the low masses range, which contributes to the largest part of the cross section. One can selects low Q^2, rejects "virtual" events of small W and a large fraction of inelastic contributions. (see figures 14 - 15).

In conclusion, I want to emphasize the fact that this process has two strong different "regime".

In the low mass range defined by the detector angular acceptance, ($w \leq 10$ GeV for H1), one observes the following caracteristics :

i) the counting rate is large ;
ii) the $e\gamma$ velocity in the Lab. is large, practically along the electron direction ;
iii) therefore, the angular acceptance in the C-of-M is limited around $\cos\theta^* \sim 0$;

iv) and the outgoing electron and photon are strongly backward in the Lab. System (generally both in the BEMC).

v) there is a large amount of acoplanar events with small w corresponding to values of Q^2 which are not small with respect to (Eγ/Ep).s.

It results that, in this range, a cut of acoplanarity is required in order to select quasi-real events and is very efficient to improve the ratio beetween elastic and inelastic contribution for luminosity measurement.

In higher mass range above 20 GeV, one notices that :

i) the counting rates strongly decrease

ii) the velocity becomes smaller, charges of direction and increases only slightly, so that

iii) the angular acceptance in the C-of-M increases and $\cos\theta^*$ becomes closer to the backward pole and

iv) the outgoing photon and electron tends to be more collinear (and coplanar) in the Lab. System with the photon in the bacward direction.

I want also notice that this work would not have been possible without the help of my friend P. Kessler.

- References -

[1] See in particular :
A. COURAU and P. KESSLER LAL 85/01 PHYS. REV. D33 (1986) 2024.
A. COURAU and P. KESSLER LAL 85/06 ; PHYS. REV.D33 (1986) 2028.
K. HAGIWARA, S. KOMAMIYA and D. ZEPPENFFELD Z. PHYS C29 (1985) 270.

[2] C. CARIMALO, P. KESSLER and J. PARISI Nucl. Phys. B57 (1973) 582-588.
G. COSME et al. Nuovo Cimento 8 (1973) 509.

[3] DELCO Coll. Phys. Lett. B 177 (1986) 109.

[4] CELLO Coll. Phys. Lett.B 168 (1986) 420.

[5] VENUS Coll. Phys. Lett.B 213 (1988) 400 .

[6] ETIM. G. PANCHERI - B. TOUSCHEK Nuovo Cimento 51B (1962) 216.
G. PANCHERI Nuovo cimento 60A (1963) 321.

MONTE CARLO FOR QED COMPTON AT HERA
WITH RADIATIVE CORRECTIONS

INTEGRATED LUMINOSITY LUM= 1.0 PICO-BARN-1
ELECTRON BEAM ENERGY EE= 30.0 GEV
PROTON BEAM ENERGY EP= 820.0 GEV
POLAR ACCEPTANCE 3.6< TETA < 176.0 DEGREES

VARIOUS CUTS :

TR.MOMENTUM : SUM(PT)< 100.00 GEV
ACOPLANARITY : |π - D(PHI)|< 45.00 DEGREE
ELECTRON ENERGY : E(EL)> 2.00 GEV
PHOTON ENERGY : E(PH)> 2.00 GEV
VISIBLE ENERGY : E(EL)+E(PH)> 20.00 GEV

CROSS-SECTIONS

ELASTIC		1047.413	PICOBARN
INELASTIC	469.942 292.401	762.342	PICOBARN
TOTAL		1809.756	PICOBARN

CROSS SECT CONFIGURATION (PICOBARN)

		PHOTON IFE	FB2	FB1	CB3	CB2	CB1	BBE	BEMC	
E	IFE	0.00	0.00	0.00	0.77	2.06	0.05	0.07	6.56	9.51
L	FB2	0.00	0.00	0.00	0.00	0.01	0.22	0.26	2.75	3.23
E	FB1	0.00	0.48	0.00	0.01	0.21	0.58	0.39	8.85	10.53
C	CB3	0.00	0.00	0.28	0.23	0.57	0.98	0.75	23.13	25.94
T	CB2	0.00	0.00	0.18	0.36	1.24	3.31	2.05	57.05	64.20
R	CB1	0.02	0.16	0.10	0.48	1.36	3.06	4.24	92.32	101.74
O	BBE	0.06	0.00	0.12	0.37	1.18	3.12	3.11	82.73	90.69
N	BEMC	0.22	0.14	0.42	2.79	12.35	28.13	38.83	1420.55	1503.44
		0.31	0.78	1.10	5.02	18.99	39.44	49.70	1693.93	1809.7

		IFE	FB2	FB1	CB3	CB2	CB1	BBE	BEMC
E	IFE								
L	FB2								
E	FB1								
C	CB3				32.44				273.38
T	CB2								
R	CB1								
O	BBE								
N	BEMC				82.90				1420.55

		IFE	FB2	FB1	CB3	CB2	CB1	BBE	BEMC
E	IFE								
L	FB2								
E	FB1								
C	CB3				16.72				198.42
T	CB2								
R	CB1								
O	BBE				48.92				1545.22
N	BEMC								

- Table 1 -

$3.6 \leqq \Theta \leqq 176$ degrees
$|\pi - \Delta\phi| \leqq 45$ degrees
$E\gamma$, Ee $\geqslant$ 2 Gev
$E\gamma + Ee \geqq 20$ Gev

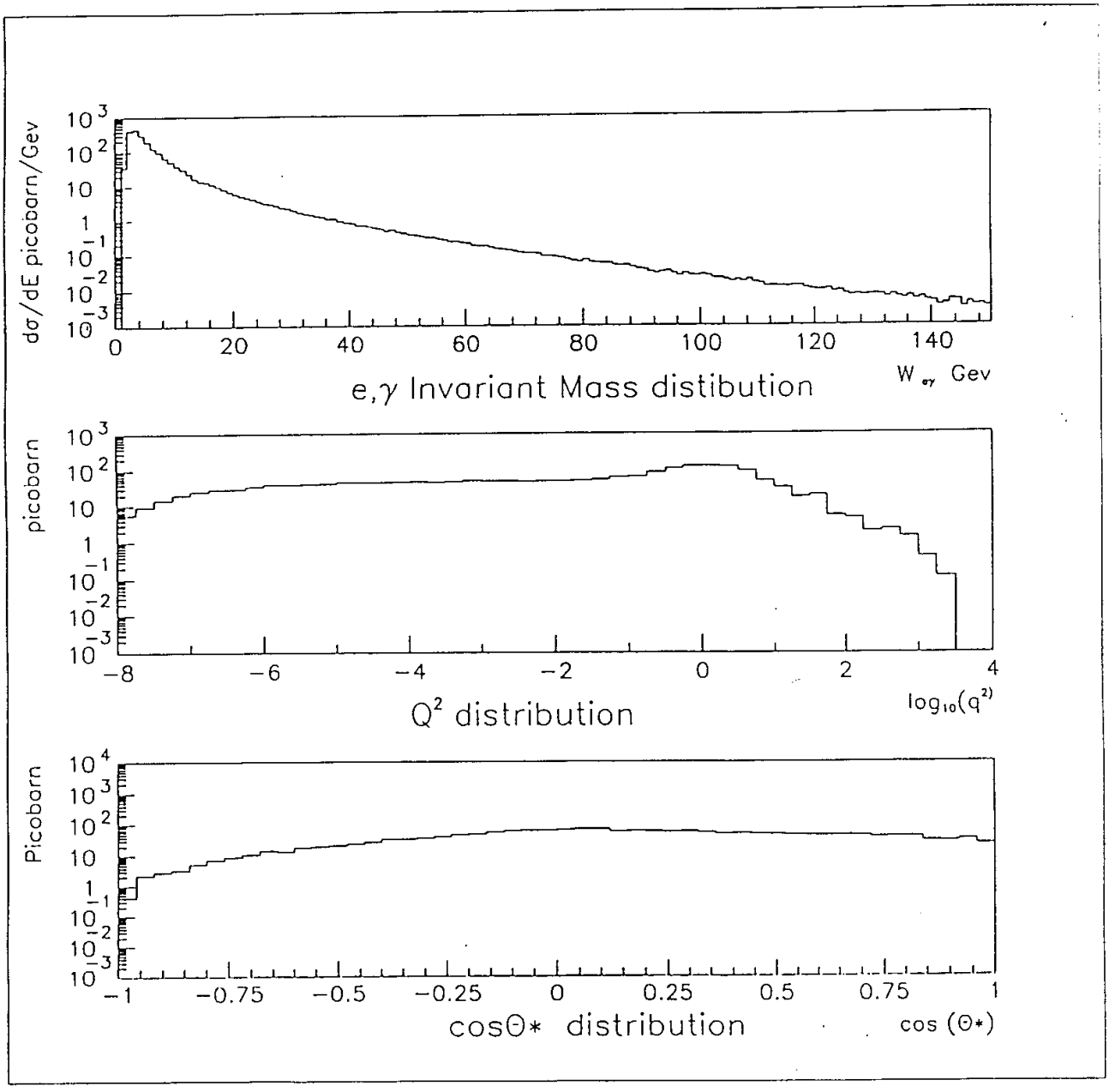

- Figure 1 -

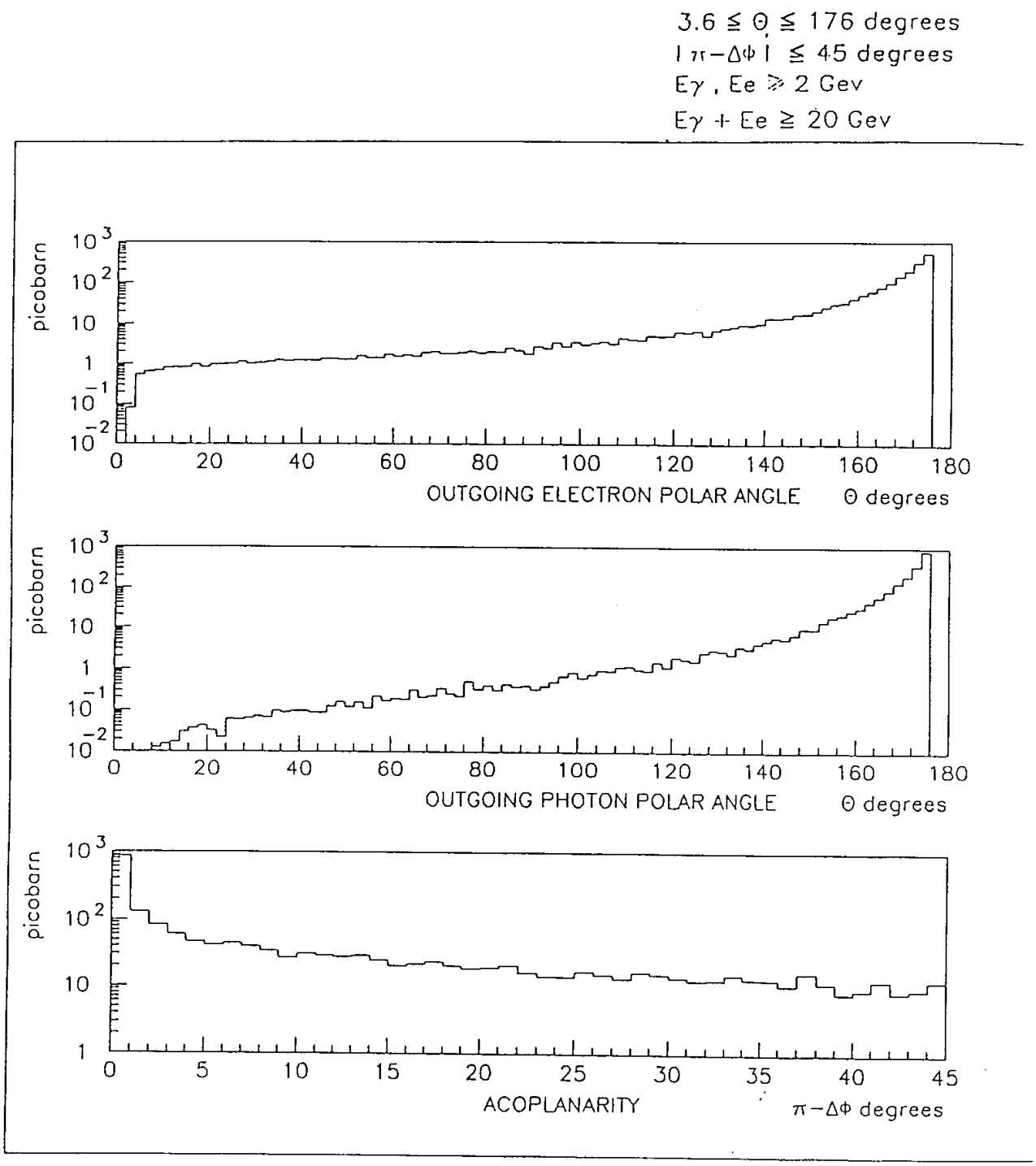
3.6 ≦ Θ ≦ 176 degrees
| π−Δφ | ≦ 45 degrees
Eγ , Ee ≫ 2 Gev
Eγ + Ee ≧ 20 Gev
picobarn
OUTGOING ELECTRON POLAR ANGLE
Θ degrees
picobarn
OUTGOING PHOTON POLAR ANGLE
Θ degrees
picobarn
ACOPLANARITY
π−Δφ degrees

- Figure 2 -

$3.6 \leqq \Theta \leqq 176$ degrees
$|\pi - \Delta\Phi| \leqq 45$ degrees
$E\gamma$, $Ee \geqslant 2$ Gev
$E\gamma + Ee \geqq 20$ Gev

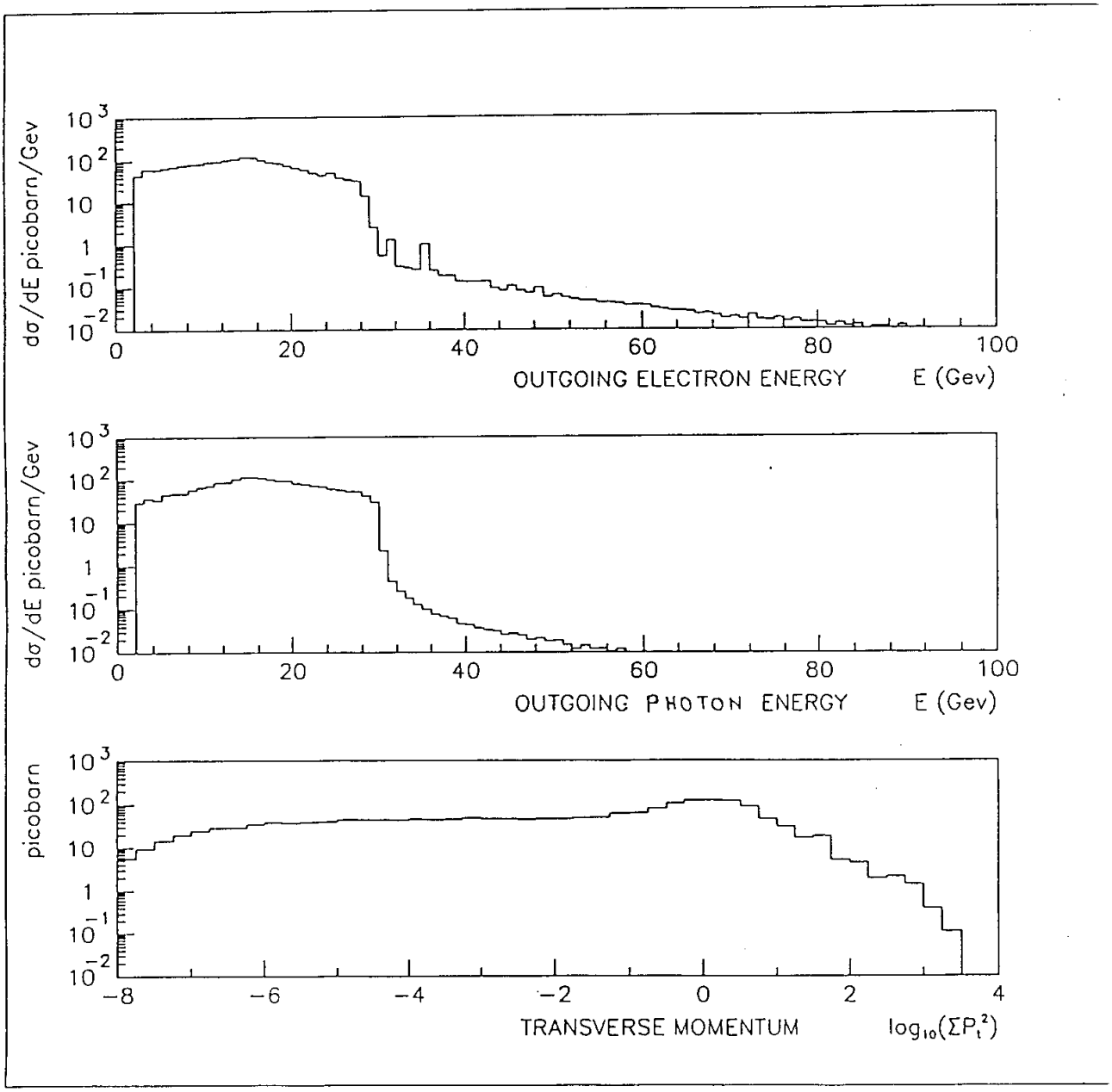

- Figure 3 -

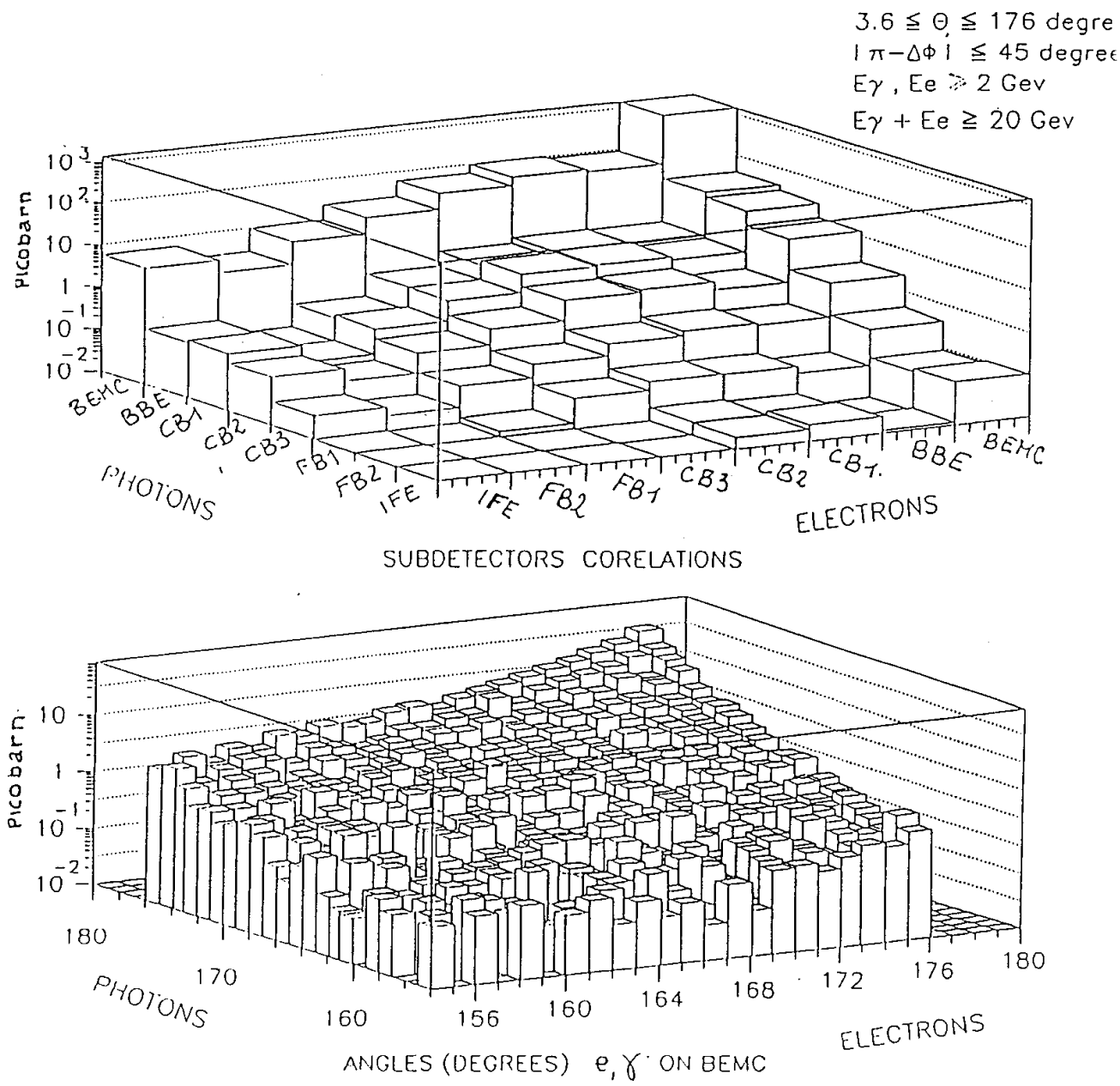
3.6 ≦ Θ ≦ 176 degre
| π−ΔΦ | ≦ 45 degree
Eγ , Ee ≥ 2 Gev
Eγ + Ee ≧ 20 Gev
Picobarn
10 3
10 2
10
1
10 -1
10 -2
BEMC
BBE
CB1
CB2
CB3
FB1
FB2
IFE
PHOTONS
IFE
FB2
FB1
CB3
CB2
CB1
BBE
BEMC
ELECTRONS
SUBDETECTORS CORELATIONS
Picobarn
10
1
10 -1
10 -2
180
170
160
156
160
164
168
172
176
180
PHOTONS
ELECTRONS
ANGLES (DEGREES) e, γ ON BEMC

- Figure 4 -

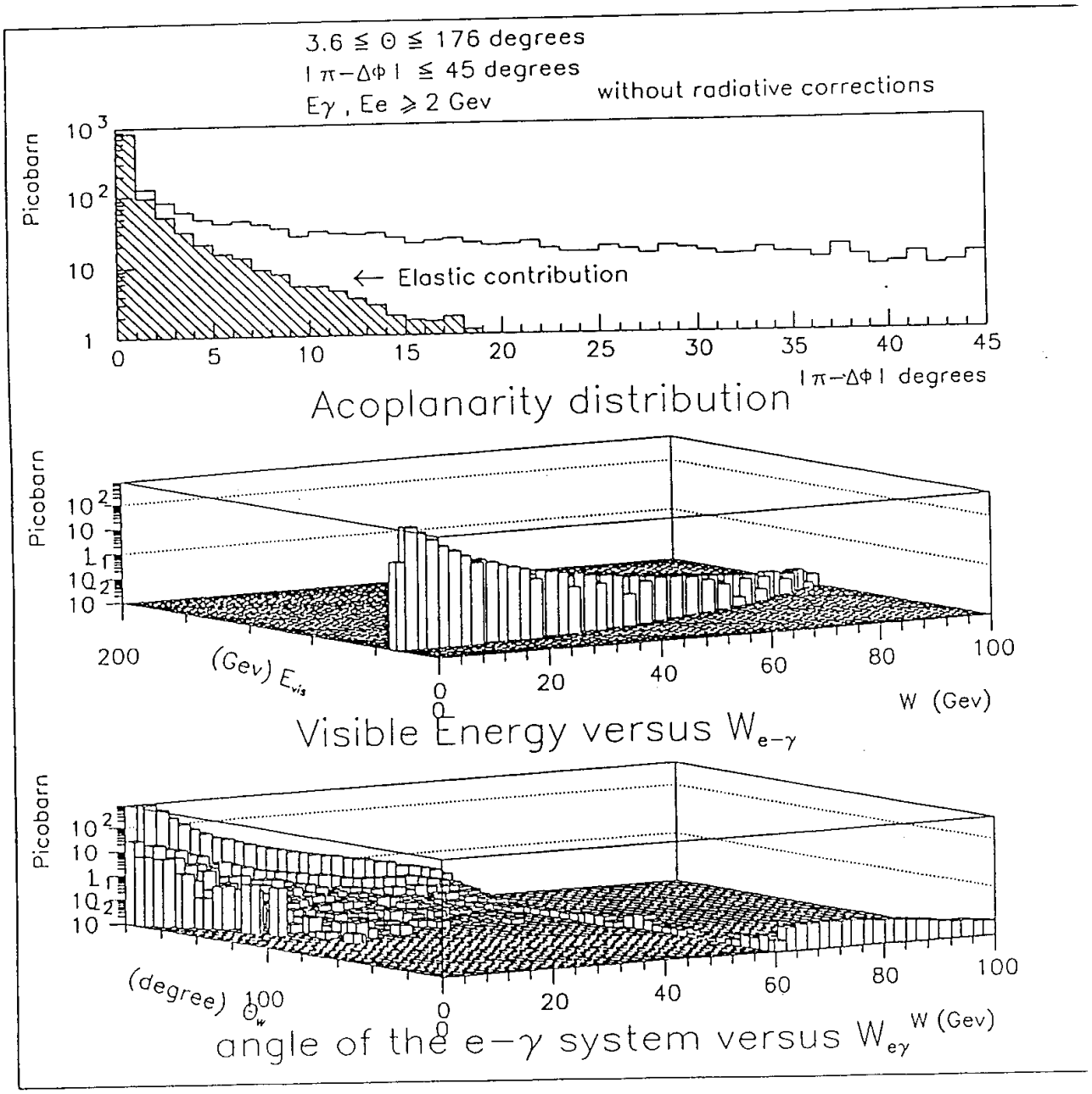
3.6 ≦ Θ ≦ 176 degrees
| π−Δφ | ≦ 45 degrees
Eγ , Ee ⩾ 2 Gev
without radiative corrections
Picobarn
← Elastic contribution
| π−Δφ | degrees
Acoplanarity distribution
Picobarn
(Gev) E_{vis}
W (Gev)
Visible Energy versus $W_{e-\gamma}$
Picobarn
(degree) θ_w
W (Gev)
angle of the e−γ system versus $W_{e\gamma}$

- Figure 5 -

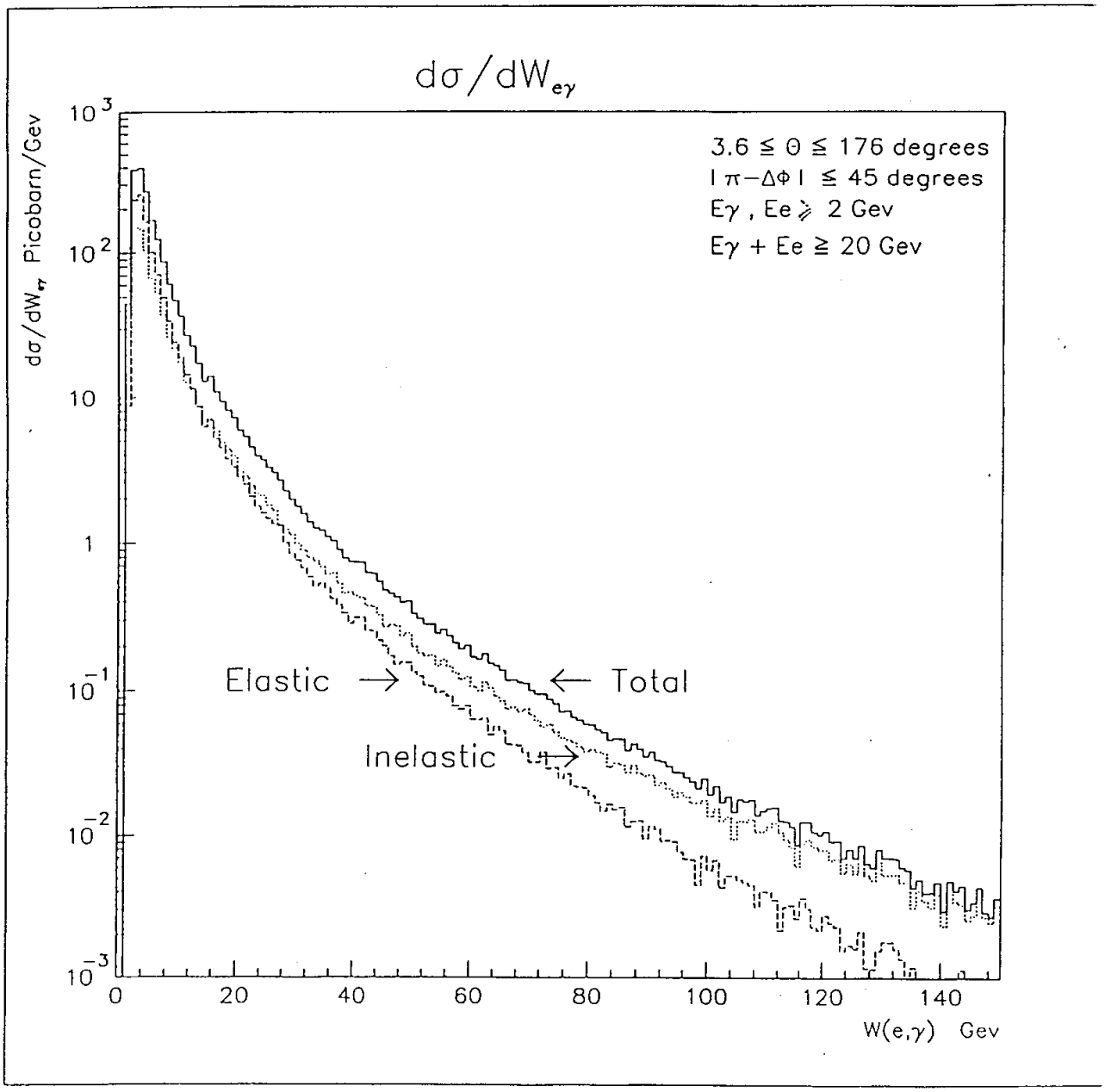
dσ/dW$_{eγ}$
3.6 ≤ Θ ≤ 176 degrees
| π−ΔΦ | ≤ 45 degrees
Eγ , Ee ⩾ 2 Gev
Eγ + Ee ≥ 20 Gev
Elastic
Total
Inelastic
dσ/dW$_{eγ}$ Picobarn/Gev
W(e,γ) Gev
10^3
10^2
10
1
10^{-1}
10^{-2}
10^{-3}
0
20
40
60
80
100
120
140

- Figure 6 -

$3.6 \leqq \Theta \leqq 176$ degrees
$|\pi - \Delta\Phi| \leqq 45$ degrees
$E\gamma$, $Ee \geqslant 2$ Gev
$E\gamma + Ee \geqq 20$ Gev

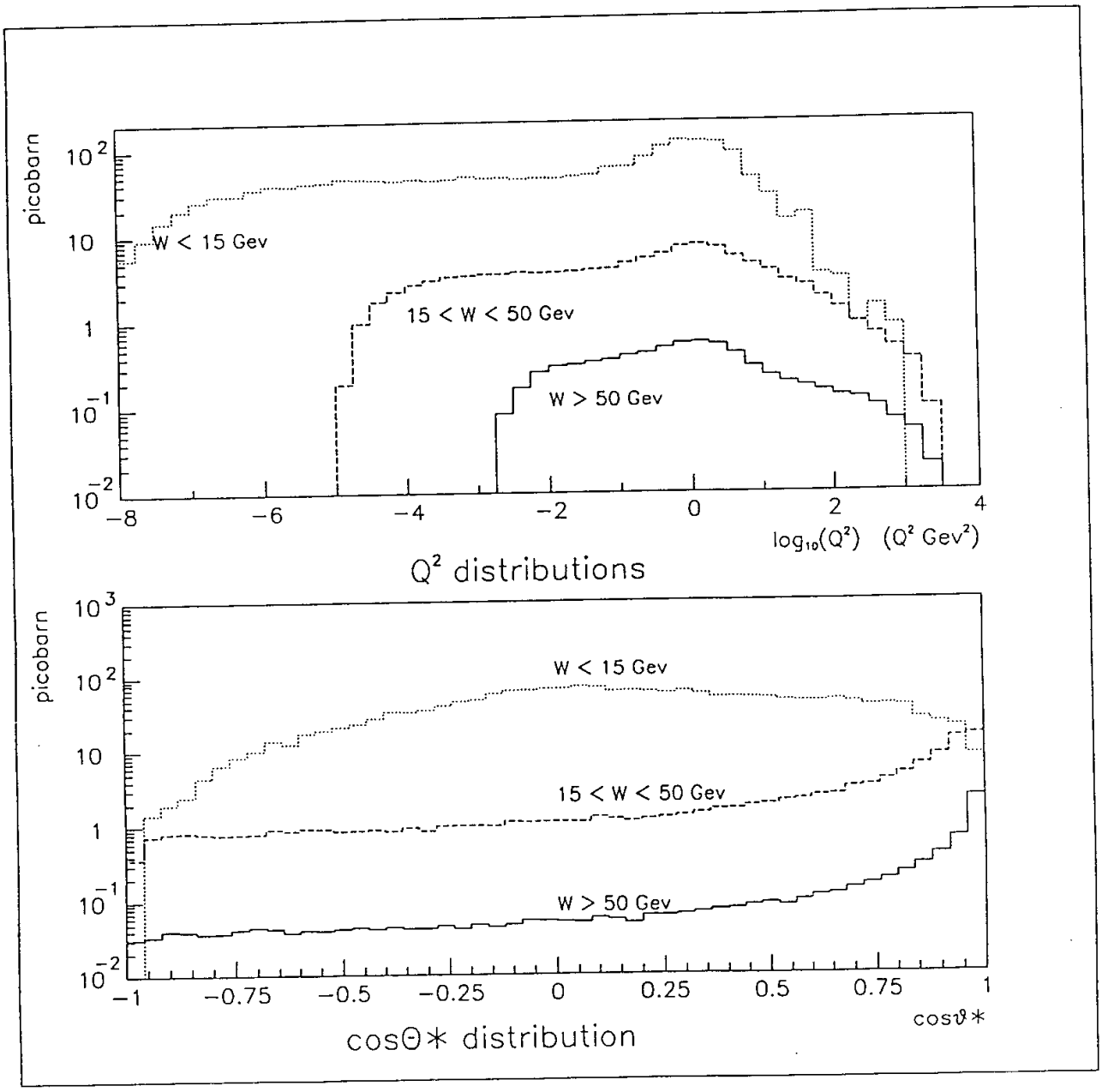

- Figure 7 -

$3.6 \leq \theta \leq 176$ degrees
$|\pi - \Delta\Phi| \leq 45$ degrees
$E\gamma$, $Ee \leq 2$ Gev
$E\gamma + Ee \geq 20$ Gev

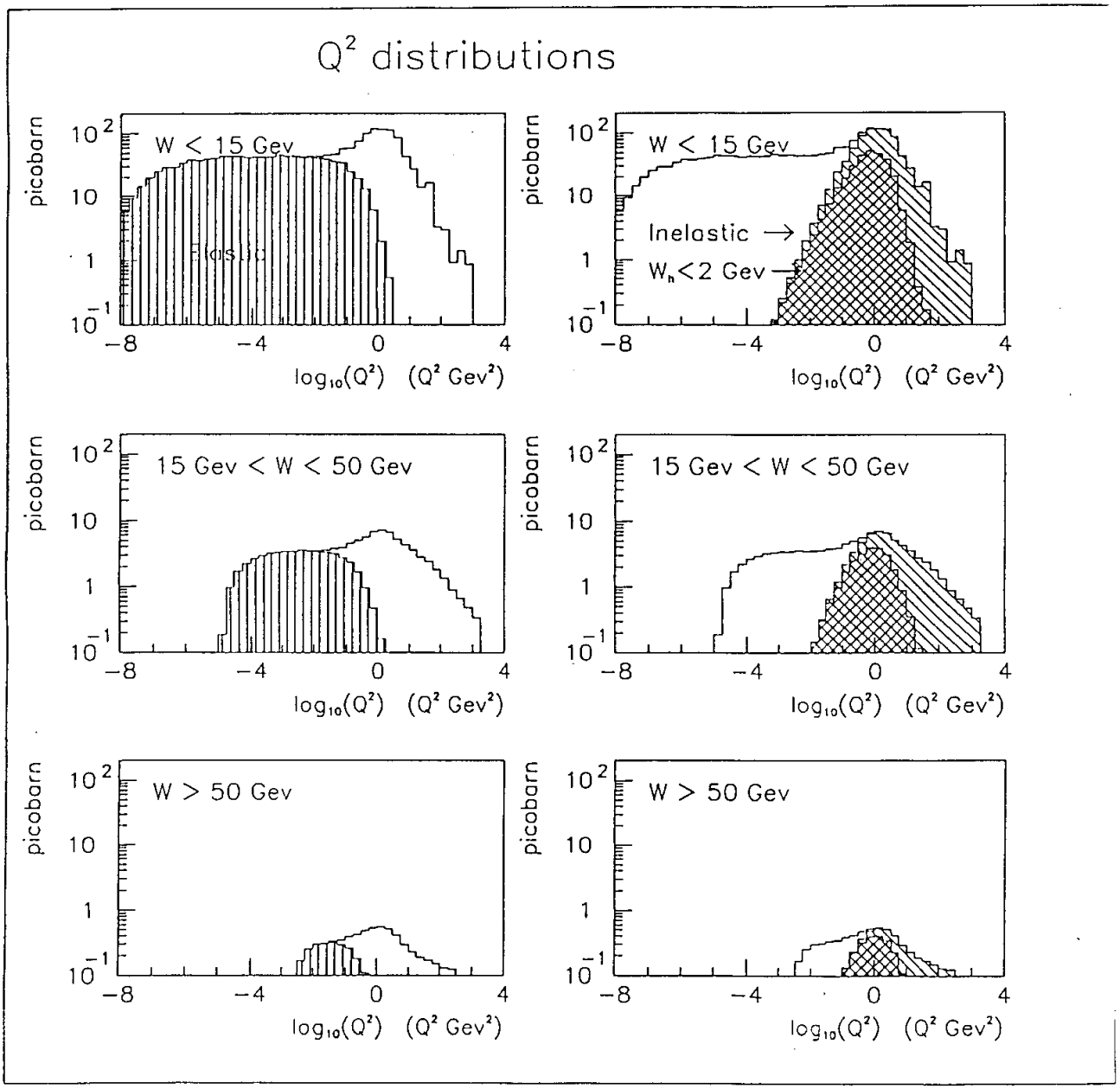

- Figure 8 -

$3.6 \leqq \theta \leqq 176$ degrees
$|\pi - \Delta\Phi| \leqq 45$ degrees
$E\gamma$, $Ee \geqslant 2$ Gev
$E\gamma + Ee \geq 20$ Gev

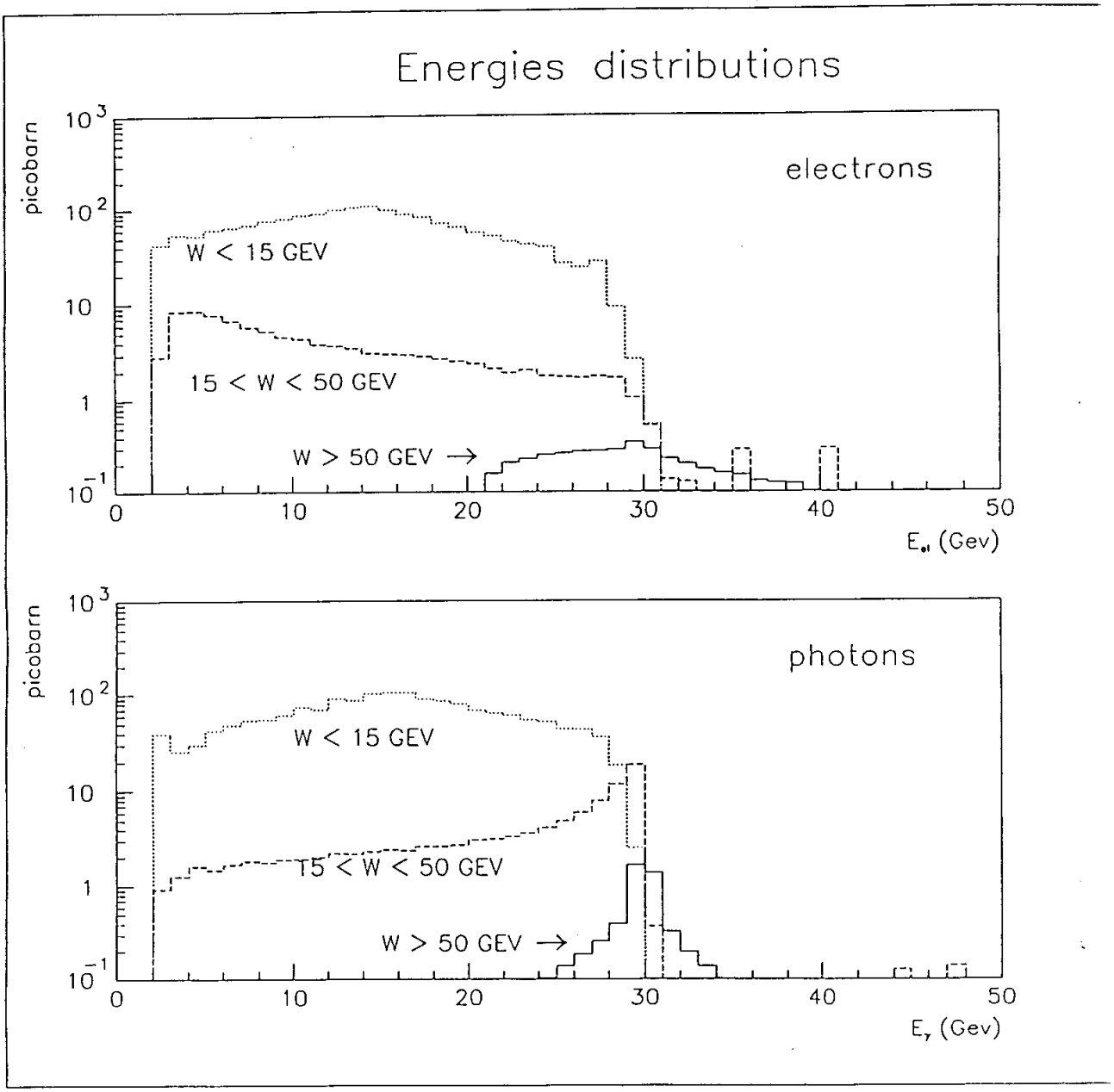

- Figure 9 - a)

$3.6 \leqq \Theta \leqq 176$ degrees
$|\pi - \Delta\Phi| \leqq 45$ degrees
$E\gamma$, Ee $\geqslant$ 2 Gev
$E\gamma + Ee \geqq 20$ Gev

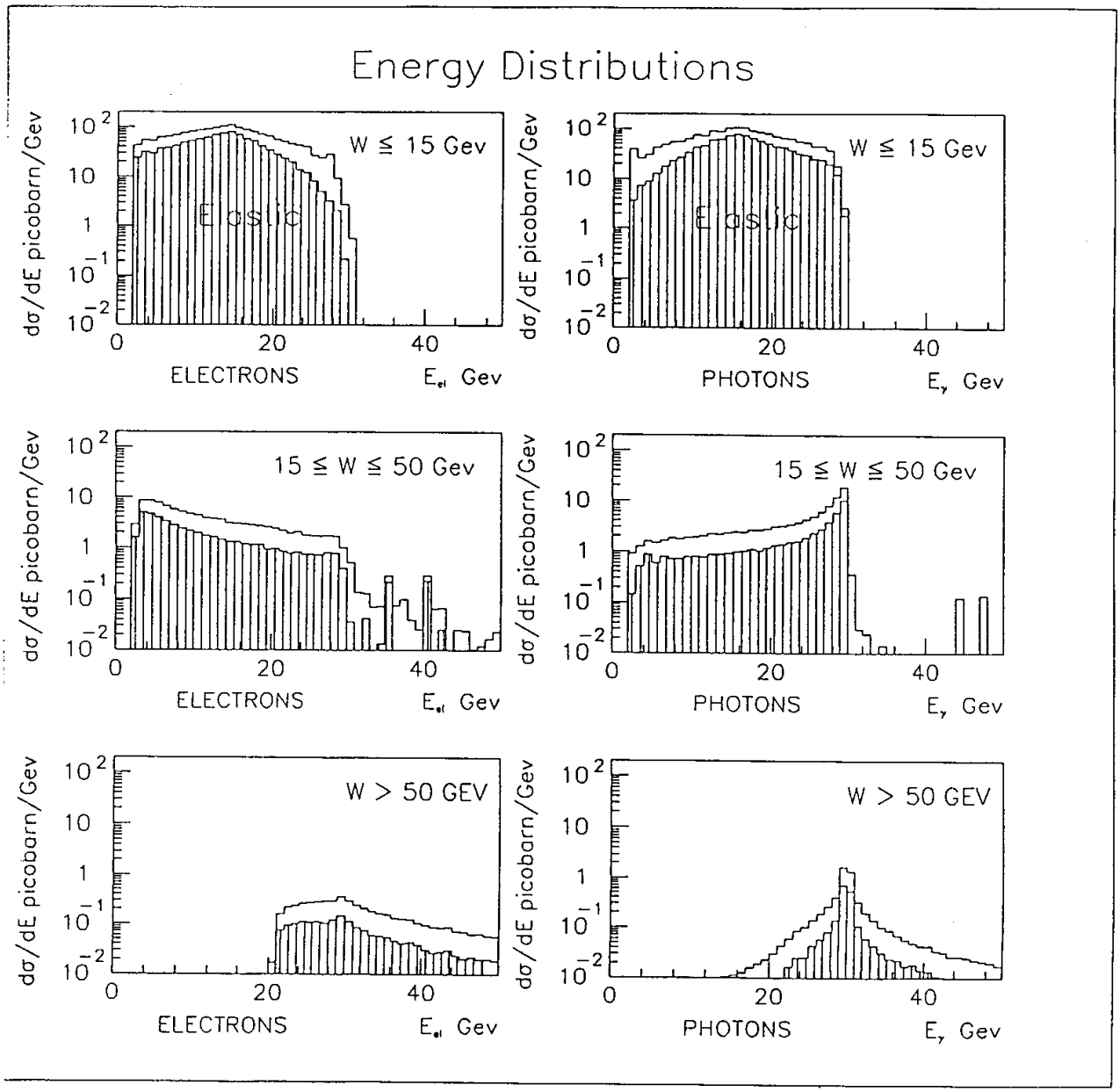

- Figure 9 -b)

$3.6 \leq \Theta \leq 176$ degrees
$|\pi - \Delta\Phi| \leq 45$ degrees
$E\gamma$, Ee $\geq$ 2 Gev
$E\gamma + Ee \geq 20$ Gev

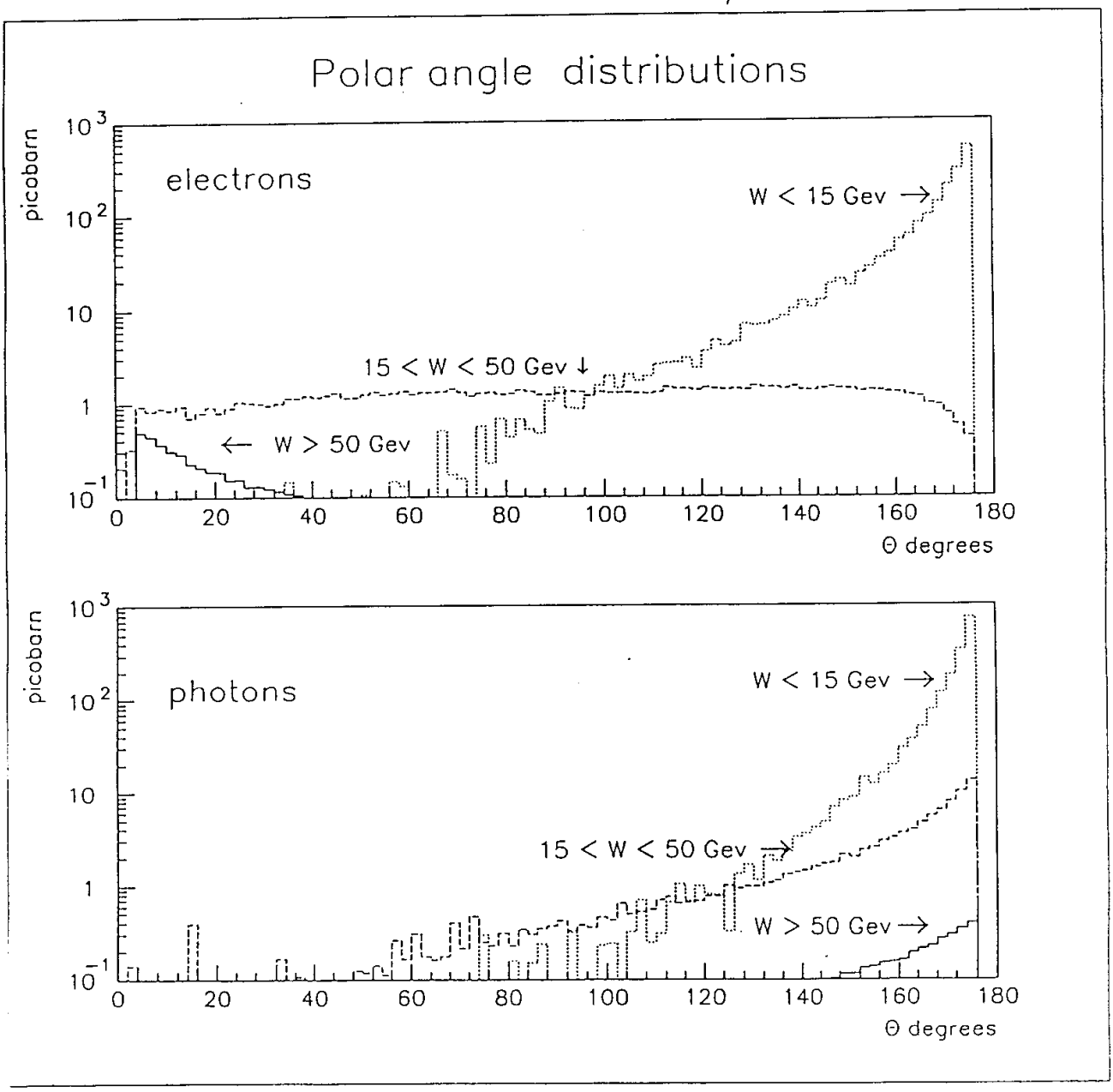

- Figure 10 - a)

$3.6 \leqq \theta \leqq 176$ degrees

$|\pi - \Delta\phi| \leqq 45$ degrees

$E\gamma$, $Ee \geqslant 2$ Gev

$E\gamma + Ee \geqq 20$ Gev

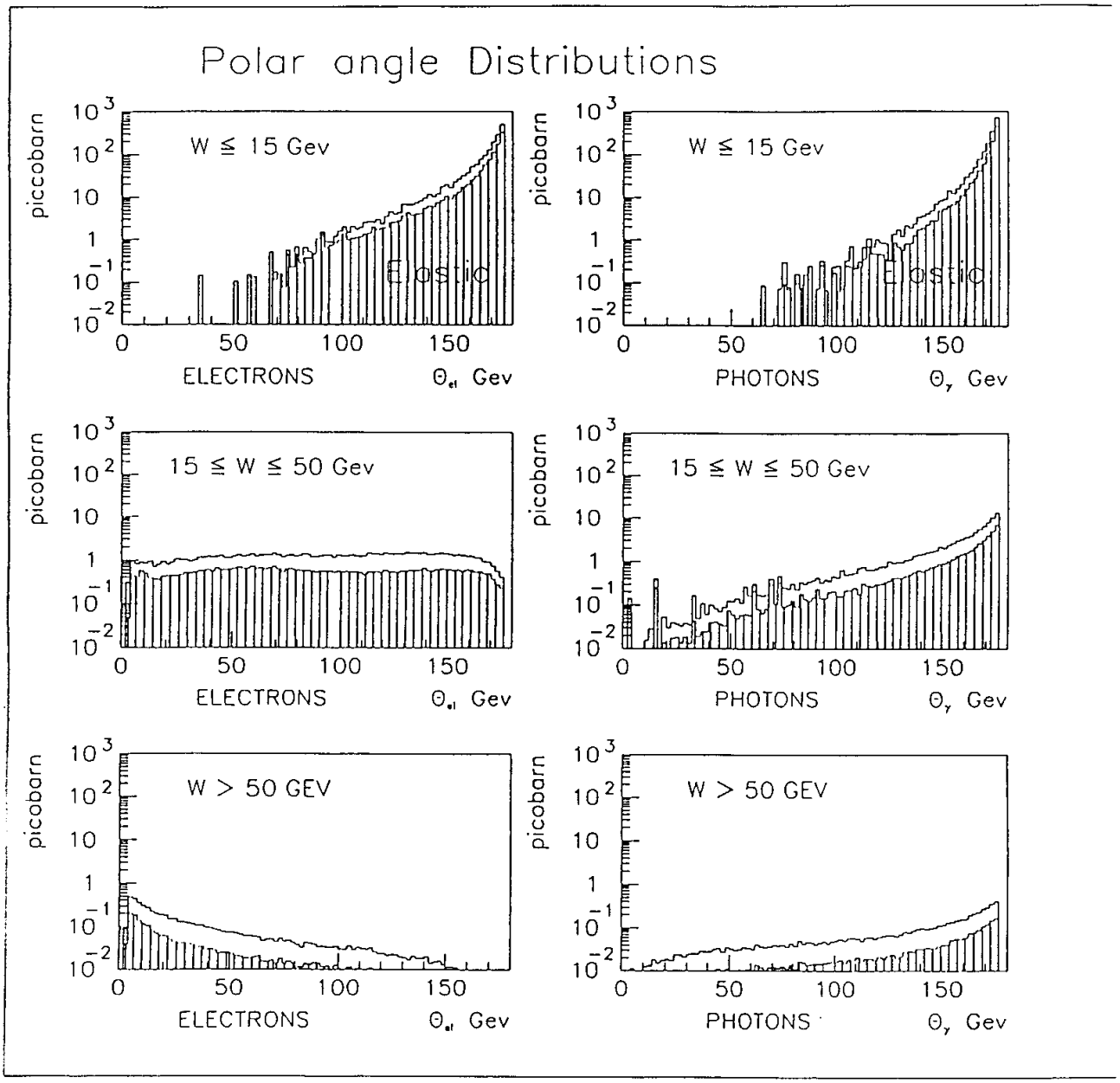

- Figure 10 - b)

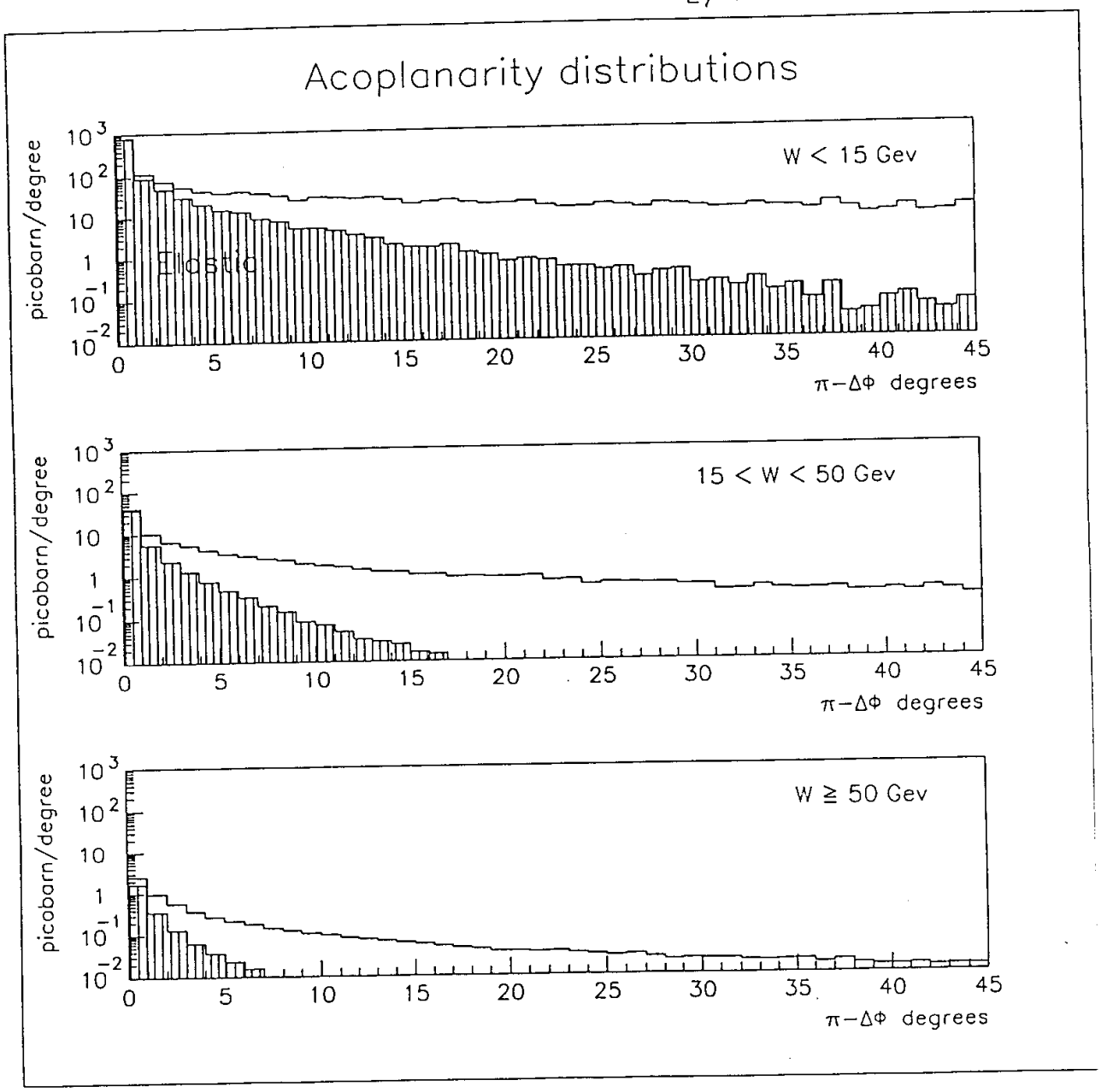
3.6 ≦ Θ ≦ 176 degrees
| π−Δφ | ≦ 45 degrees
Eγ , Ee ≧ 2 Gev
Eγ + Ee ≧ 20 Gev
Acoplanarity distributions
picobarn/degree
W < 15 Gev
Elastic
π−Δφ degrees
15 < W < 50 Gev
W ≧ 50 Gev

- Figure 11 -

3.6 ≦ Θ ≦ 176 degrees
| π−ΔΦ | ≦ 45 degrees
Eγ , Ee ≦ 2 Gev

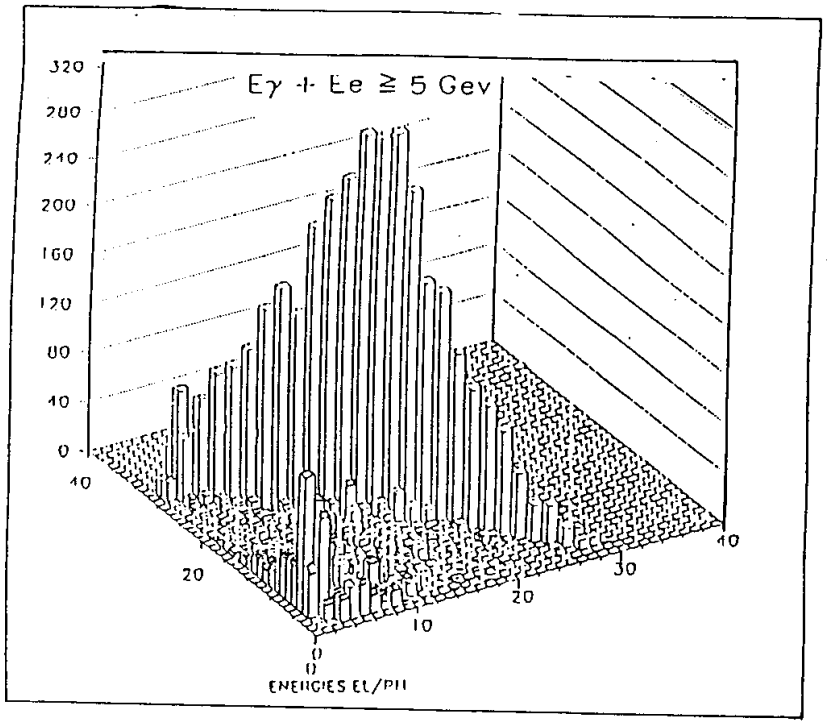

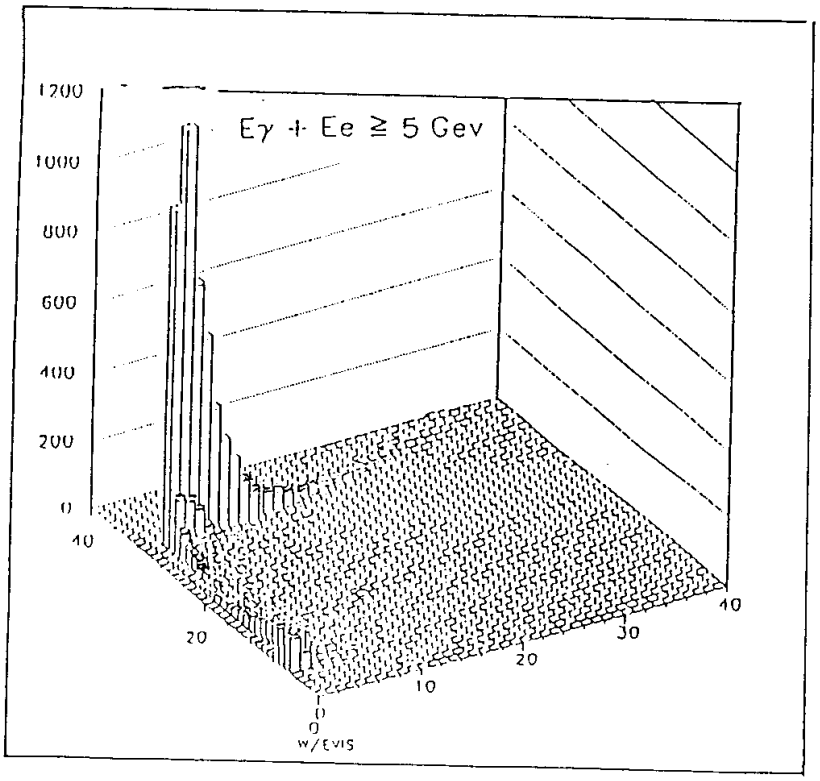

- Figure 12 -

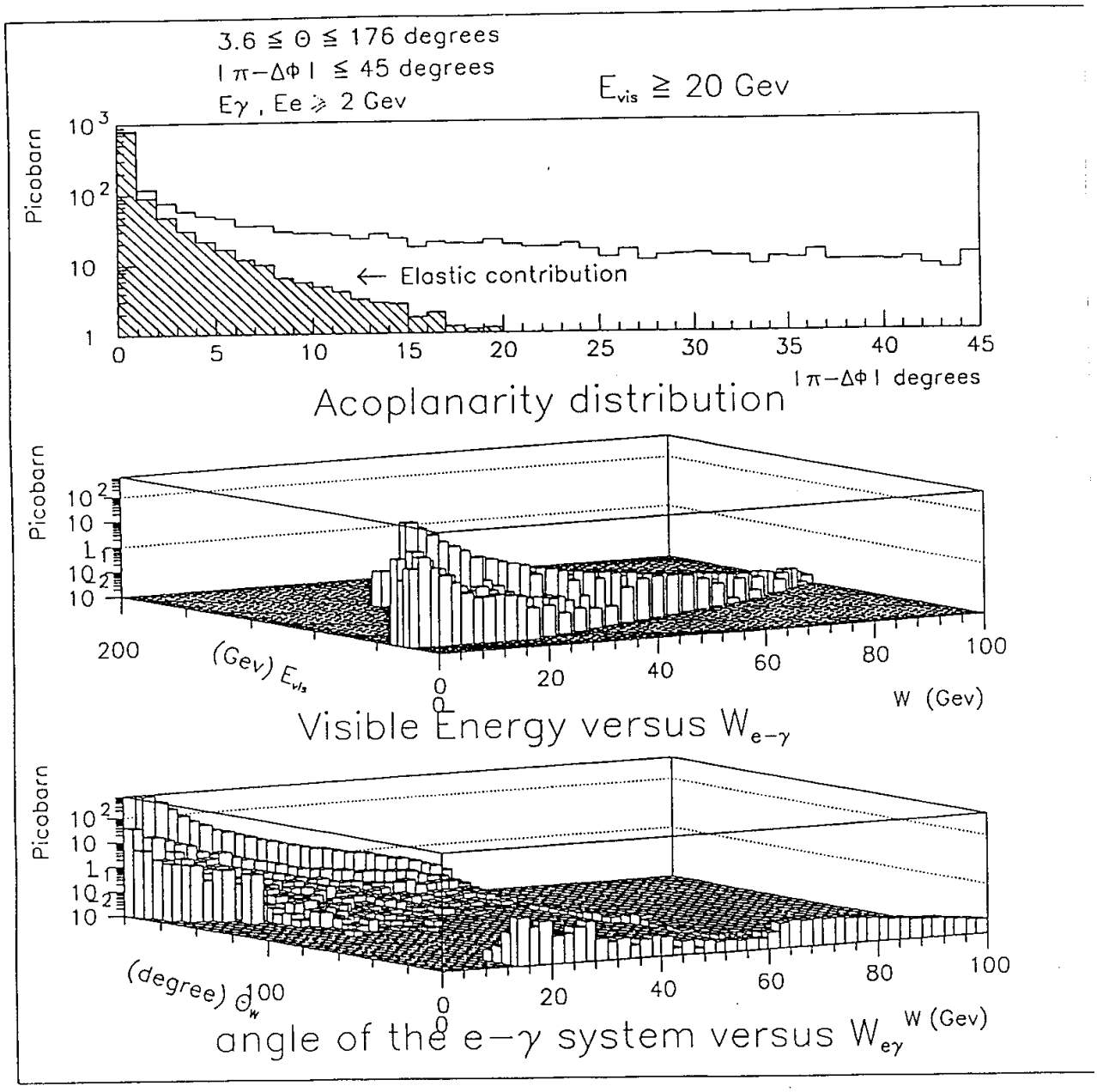
3.6 ≦ Θ ≦ 176 degrees
| π−Δφ | ≦ 45 degrees
Eγ , Ee ≫ 2 Gev
E_{vis} ≧ 20 Gev
Picobarn
← Elastic contribution
| π−Δφ | degrees
Acoplanarity distribution
Picobarn
(Gev) E_{vis}
W (Gev)
Visible Energy versus $W_{e-\gamma}$
Picobarn
(degree) Θ_w
W (Gev)
angle of the e−γ system versus $W_{e\gamma}$

- Figure 13 -

$3.6 \leq \theta \leq 176$ degrees

$E\gamma$, $Ee \geq 2$ Gev

$E\gamma + Ee \geq 20$ Gev

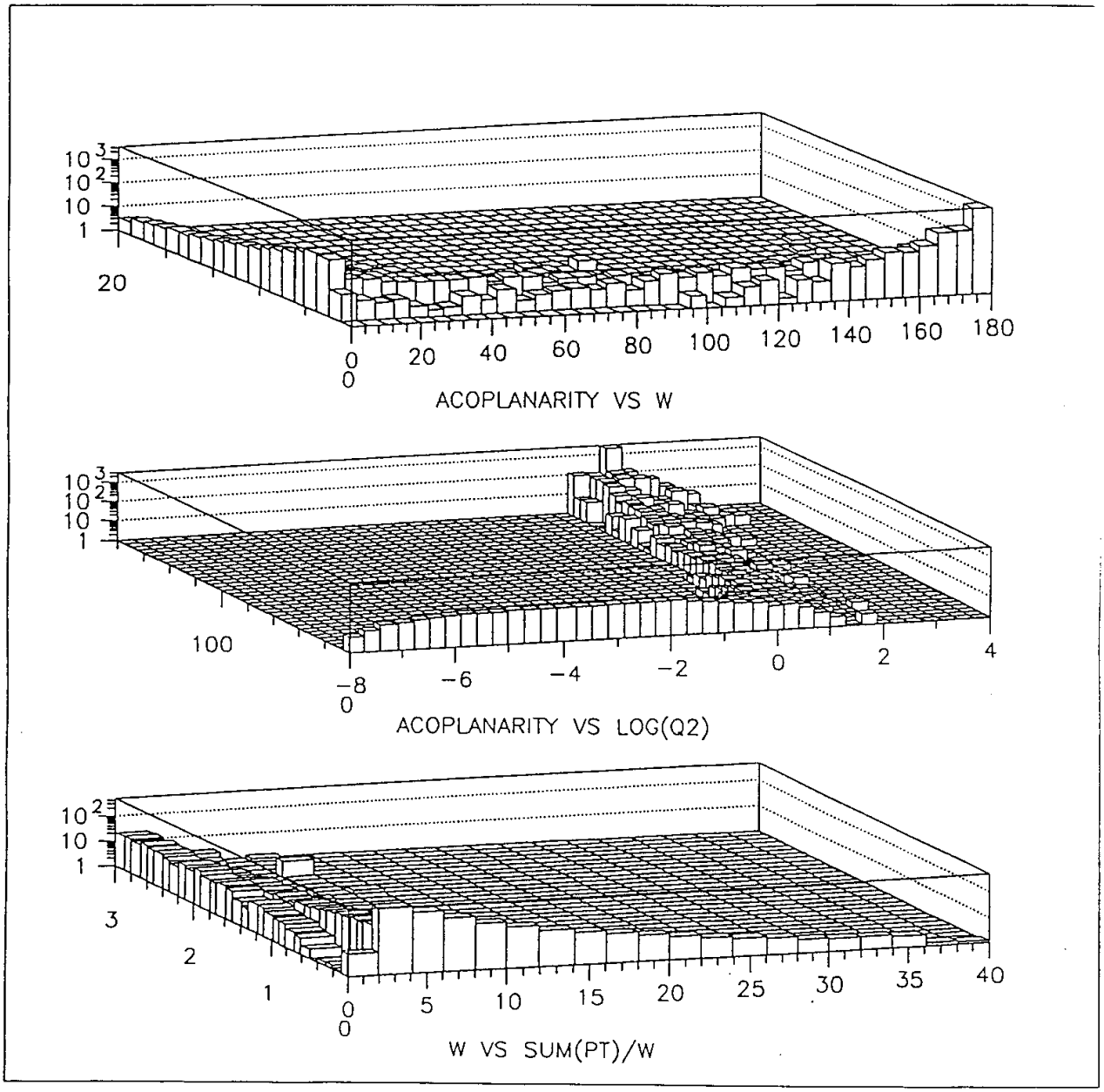

- Figure 14-

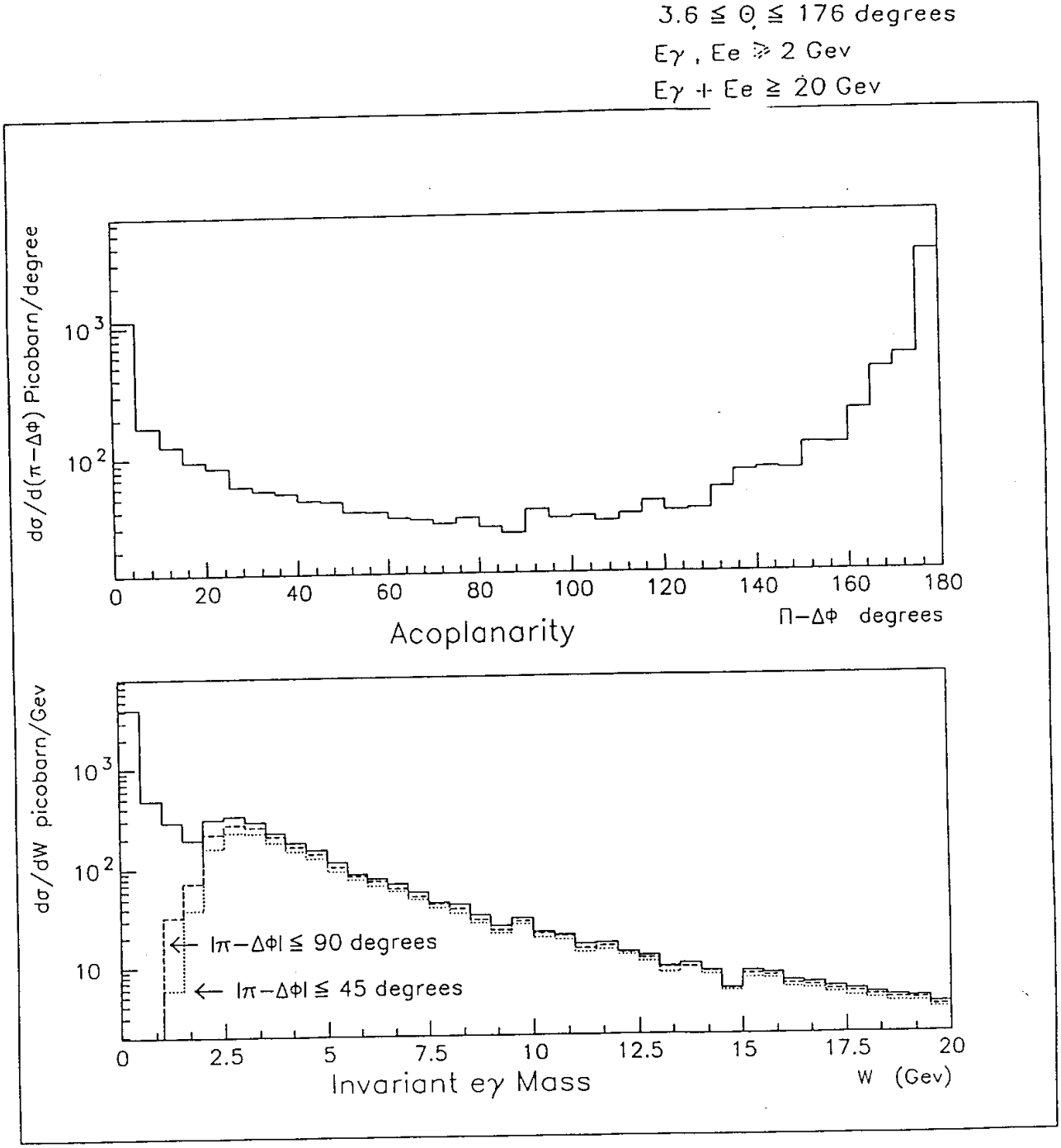
3.6 ≦ Θ ≦ 176 degrees
Eγ , Ee ≧ 2 Gev
Eγ + Ee ≧ 20 Gev
dσ/d(π−Δφ) Picobarn/degree
10³
10²
0
20
40
60
80
100
120
140
160
180
Acoplanarity
Π−Δφ degrees
dσ/dW picobarn/Gev
10³
10²
10
|π−Δφ| ≦ 90 degrees
|π−Δφ| ≦ 45 degrees
0
2.5
5
7.5
10
12.5
15
17.5
20
Invariant eγ Mass
W (Gev)

- Figure 15 -